Nanoscale Research Letters

NANO EXPRESS

Open Access

An Ultrathin, Triple-Band Metamaterial Absorber with Wide-Incident-Angle Stability for Conformal Applications at X and Ku Frequency Band

Guangsheng Deng[1], Kun Lv[1], Hanxiao Sun[1], Jun Yang[1*], Zhiping Yin[1], Ying Li[1], Baihong Chi[2] and Xiangxiang Li[3]

Abstract

An ultrathin and flexible metamaterial absorber (MA) with triple absorption peaks is presented in this paper. The proposed absorber has been designed in such a way that three absorption peaks are located at 8.5, 13.5, and 17 GHz (X and Ku bands) with absorption of 99.9%, 99.5%, and 99.9%, respectively. The proposed structure is only 0.4 mm thick, which is approximately 1/88, 1/55, and 1/44 for the respective free space wavelengths of absorption frequency in various bands. The MA is also insensitive due to its symmetric geometry. In addition, the proposed structure exhibits minimum 86% absorption (TE incidence) within 60° angle of incidence. For TM incidence, the proposed absorber exhibits more than 99% absorptivity up to 60° incidence. Surface current and electric field distributions were investigated to analyze the mechanism governing absorption. Parameter analyses were performed for absorption optimization. Moreover, the performance of the MA was experimentally demonstrated in free space on a sample under test with 20 × 30 unit cells fabricated on a flexible dielectric. Under normal incidence, the fabricated MA exhibits near perfect absorption at each absorption peak for all polarization angles, and the experimental results were found to be consistent with simulation results. Due to its advantages of high-efficiency absorption over a broad range of incidence angles, the proposed absorber can be used in energy harvesting and electromagnetic shielding.

Keywords: Metamaterial, Absorber, Conformal, Ultrathin, Multi-band

Introduction

In recent years, metamaterials have received widespread concern due to their exotic properties, such as negative refractive index [1], perfect imaging [2], and inverse Doppler effects [3]. Because of these properties, metamaterials have been proposed for use in various devices, such as electromagnetic (EM) cloaking [4], ultra-sensitive sensing [5], filters [6, 7], and absorbers [8–12]. In particular, metamaterial absorbers (MAs), compared with traditional microwave absorbers, are used in a variety of fields, ranging from military to consumer electronics. MAs tend to be lightweight and thin.

In 2008, a perfect MA was first presented by Landy et al. [13]. Subsequently, different types of MAs, such as single-band [14, 15], dual-band [16–21], multi-band [22–27], and wideband absorbers [28–36], have been presented by various researchers. Among these MAs, multi-band MAs enable perfect absorption at several discrete frequencies, enabling applications like multiband sensing. In general, a multi-band MA can be configured with two methods. The first method is commonly known as the coplanar construction method, where several resonators of different sizes are formed into a super-unit

*Correspondence: junyang@hfut.edu.cn
[1] Special Display and Imaging Technology Innovation Center of Anhui Province, Academy of Opto-Electronic Technology, Hefei University of Technology, Hefei 230009, China
Full list of author information is available at the end of the article

structure [37, 38]. The second method involves vertical stacking of alternating multi-layer structures [39, 40]. However, neither of these methods is ideal for fabricating a structure that provides multiband absorption. For example, coplanar construction method leads to an inevitably expanding of the MA unit size, whereas the layered design could not eliminate the disadvantage of large thickness and heavy weight of the structure. Recently, some simplified structural designs were presented to achieve multi-band absorption [41, 42]; nevertheless, the absorption at wide incident angle still needs to be improved.

In this paper, we propose a design method that combines the advantage of compact-size, ultra-thin, lightweight, and easy-to-fabricate. In merit of the unit cell design, the proposed triple-band MA exhibits high absorption even at wide angles of incidence. Simulation results reveal three distinct absorption bands with peak absorption of 99.9%, 99.5%, and 99.9% at 8.5, 13.5, and 17 GHz, respectively. The symmetric structure of the MA ensures its absorption is insensitive to different polarization angles. Moreover, the proposed MA offers absorption greater than 86% and 99% when TE and TM-polarized waves are incident at 60° angle of incidence, respectively. The relationship between various geometric parameters and the absorption spectrum was examined. To validate the absorbing performance of the MA, a prototype with 20×30 unit cells was fabricated, and the experimental results are found to be consistent with simulation results. Due to its low thickness and effectiveness for a broad range of incident angles, the MA structure was fabricated on a highly flexible polyimide film, which can be used in non-planar and conformal applications.

Methods/Experimental

Figure 1 shows the geometry of the unit cell for the proposed MA, which consists of a resonance layer, a dielectric layer, and a metallic ground layer. The resonant structure combines a split ring resonator (SRR), a modified ring resonator (MRR), and eight identical 7-shaped structures, each rotated 45° along the unit' center. The top patterned layer and bottom ground layer are made of 0.02-mm-thick copper and an electric conductively of 5.8×10^7 S/m. The substrate was fabricated on polyimide with relative permittivity of 2.9 and loss tangent of

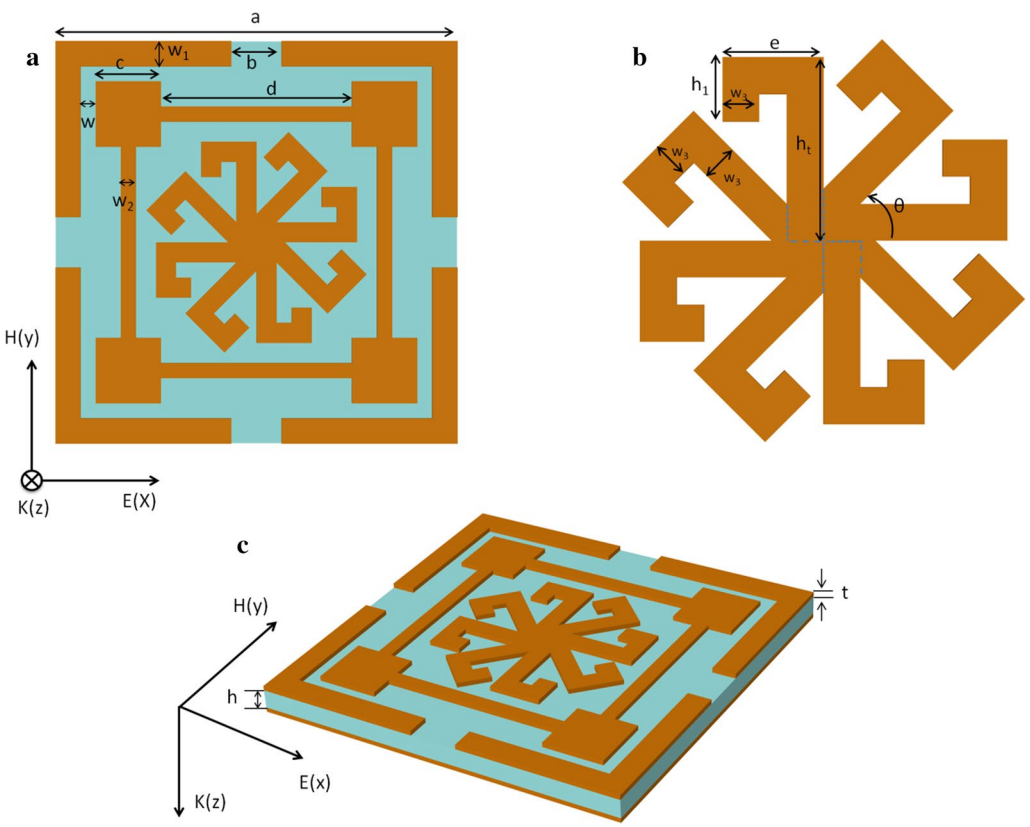

Fig. 1 Schematic geometry of a unit cell for the proposed MA. **a** Top view, **b** layout of the eight 7-shaped resonance structures, and **c** perspective view of a unit cell

0.02. The optimized parameters of the MA are listed in Table 1.

The simulated absorption spectra of the proposed MA were determined from a finite-difference time-domain (FDTD) simulation. In the simulation, the unit cell boundary conditions were applied in the x and y directions, while the Floquet port condition was imposed along the z direction. Moreover, a plane EM wave was assumed to hits the surface of the MA. The absorptivity (A) can be defined as $A(\omega) = 1 - |S_{11}(\omega)|^2 - |S_{21}(\omega)|^2$, where $S_{11}(\omega)$ and $S_{21}(\omega)$ are the reflection and the transmission coefficients, respectively. Since the transmission coefficient $S_{21}(\omega)$ is zero due to the total reflection of copper ground plane, the absorptivity can be simplified as $A(\omega) = 1 - |S_{11}(\omega)|^2$. The simulated reflection and absorption spectra of the proposed MA under normal incidence are shown in Fig. 2a. The proposed MA exhibits three absorption peaks at 8.5, 13.5, and 17 GHz with absorption of 99.9%, 99.5%, and 99.9%, respectively; the corresponding Q factor of each resonant mode can reach 26.8, 28.4, and 27.1, respectively.

Table 1 Dimensions and parameters of the MA

Parameter	Value (mm)	Parameter	Value (mm)
a	8	w_2	0.3
b	1	w_3	0.5
c	1.3	h	0.4
d	3.8	h_1	0.7
e	1.2	h_t	2
w	0.3	t	0.02
w_1	0.5	θ	45°

Figure 2b shows the absorption spectra of the proposed MA structure for different polarization angles. One can see that the absorption of the MA remains stable for polarization angle ranging from 0° to 90°. Therefore, the proposed MA is insensitive to polarization of incident EM waves. In addition, we further investigated absorption in the designed MA at oblique angle of incidence (θ). For TE polarization, as shown in Fig. 2c, the absorptivity

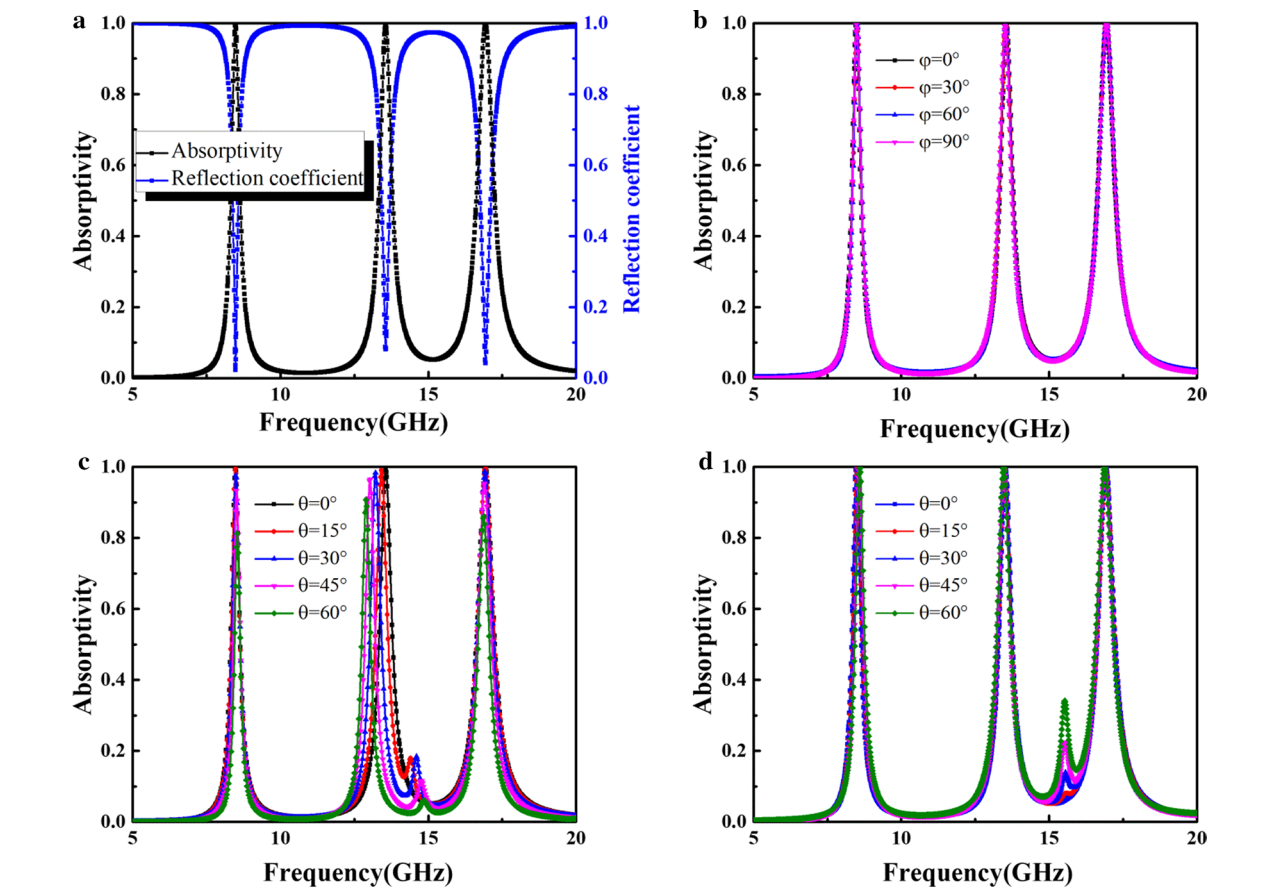

Fig. 2 **a** Simulated absorption and reflection spectra at normal incidence. **b** Absorption spectrum for different polarization angles φ. Absorption for different θ values for **c** TE and **d** TM polarization

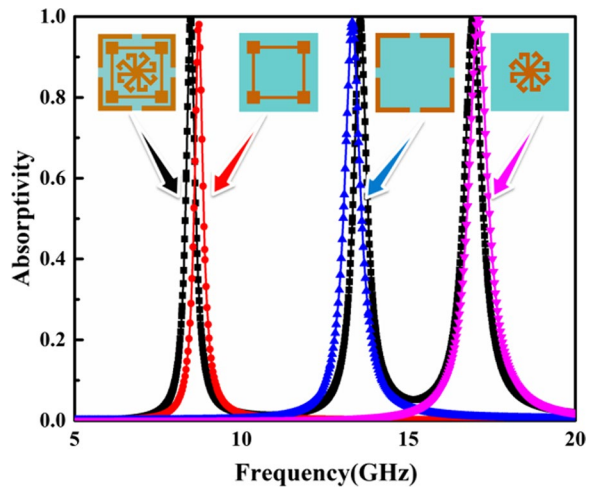

Fig. 3 Contribution from individual elements to absorption

decreases as θ increases. This may occur because increasing θ decreases the horizontal component of the electric field intensity for TE waves. Therefore, the effectiveness of the circulating current generated by the incident electric field gradually decreases. However, the three absorption peaks remain above 86% as θ reach up to 60°. For TM polarization, as shown in Fig. 2d, the absorptivity at each resonance peak is greater than 99% at $\theta = 60°$. This occurs because absorption in the proposed MA is less sensitive to changes in the electric field intensity caused by an increase in θ. Another advantage of the proposed MA is the absorption frequency stability, as shown in Fig. 2, where the three distinct absorption peaks do not change significantly as θ increases.

Results and Discussion

In order to facilitate a detailed explanation of absorption, the response spectra for different parts of the resonance structure are presented in Fig. 3. As shown in Fig. 3, each element within the patterned layer is responsible for an individual and intense resonance. As a result, a combination of these elements leads to perfect multiband absorption. As part of the MRR design, a square patch is added to each corner of the closed ring resonator, which increases the electrical length of the ring resonator and red-shifts the absorption frequency without increasing the size of the structure.

To further explore the mechanism of EM wave absorption, surface current density distributions on the top and bottom metallic layers corresponding to three absorption peaks are shown in Fig. 4. One can see that the surface

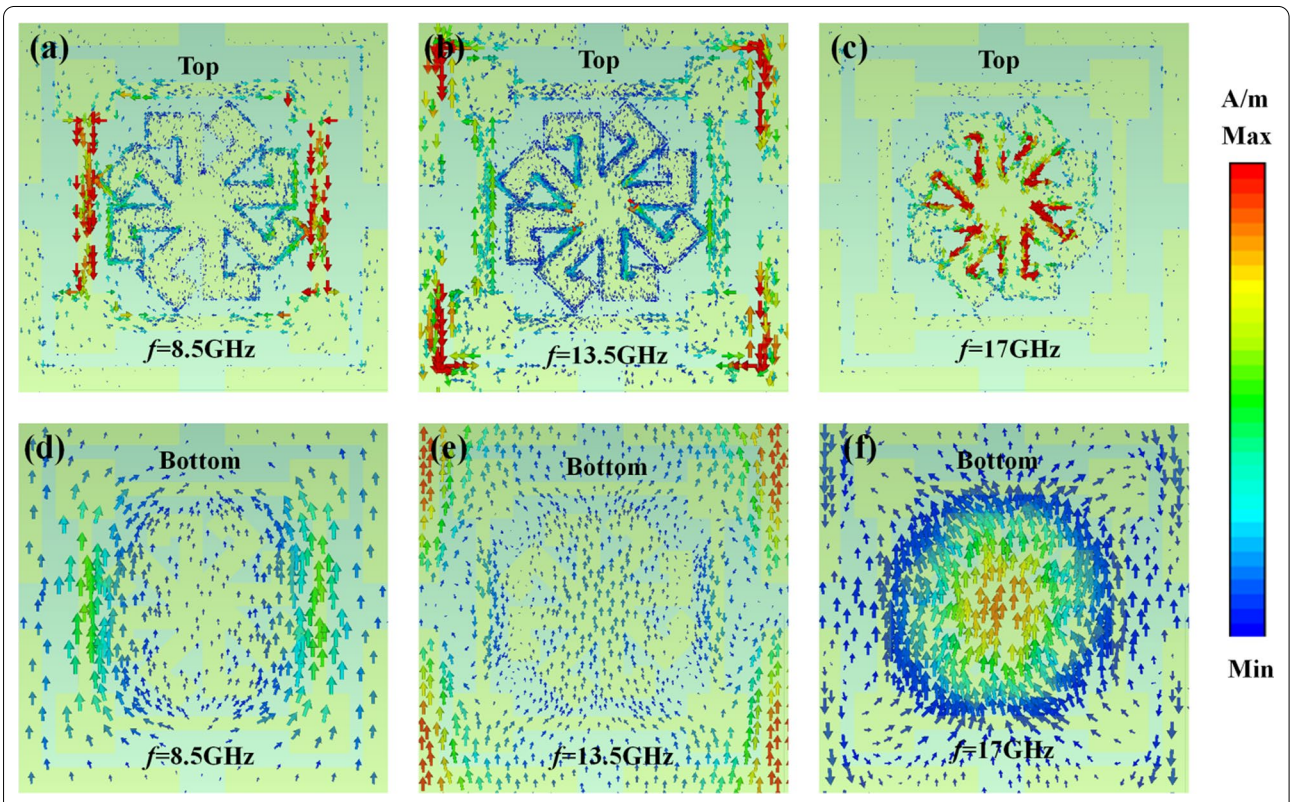

Fig. 4 Simulated surface current distribution on the top patterned layer and bottom ground layer at **a**, **d** 8.5, **b**, **e** 13.5, and **c**, **f** 17 GHz

current on the top patterned layer is concentrated on the MRR, the SRR, and the 7-shaped graphic structures at 8.5, 13.5, and 17 GHz, respectively. The surface current distribution also reveals the origin of wave absorption, as shown in Fig. 3. Compared with the surface current on the top layer, the intensity on the bottom ground layer is much weaker. The direction of the surface current on top layer is anti-parallel with respect to ground plane, which results in equivalent current loops within the MA that excites a magnetic dipole. Meanwhile, Fig. 5 shows the amplitude of the electric field ($|E|$) in the MA for incident TE-polarization waves when $\theta = 0°$, 30°, and 60°. One can see that the electric field is strongly concentrated on the horizontal bars of the MRR as the MRR absorbs at 8.5 GHz. At 13.5 GHz, as shown in Fig. 5(b), perfect absorption is due to the LC resonance in the SRR. Finally, absorption at 17 GHz is due to a dipole resonance in the inner patch. The resonators in the top layer also develop electric resonances. Both the magnetic and electric resonances contribute to strong EM absorption in the proposed structure. In addition, Fig. 5 shows that the field intensity decrease as θ increases. As a result, EM wave absorption also decreases with the increase of θ.

Figure 6 shows the effects of the MA geometry on absorption in the proposed MA. As shown in Fig. 6a, the resonant frequencies shift toward higher frequencies as

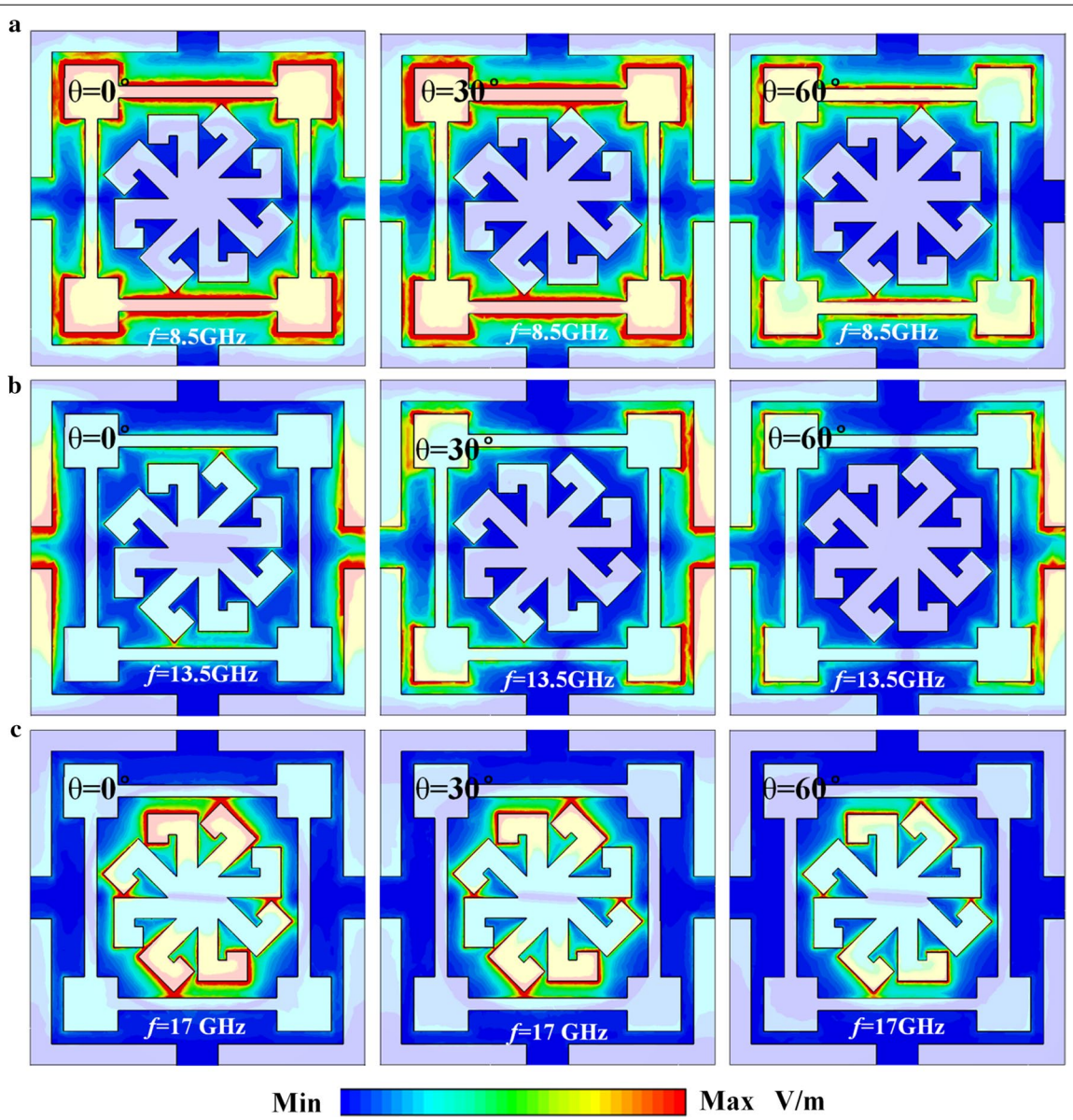

Fig. 5 The absolute of electric field distribution ($|E|$) in the MA for TE polarization at different incident angle θ of **a** 8.5, **b** 13.5, and **c** 17 GHz

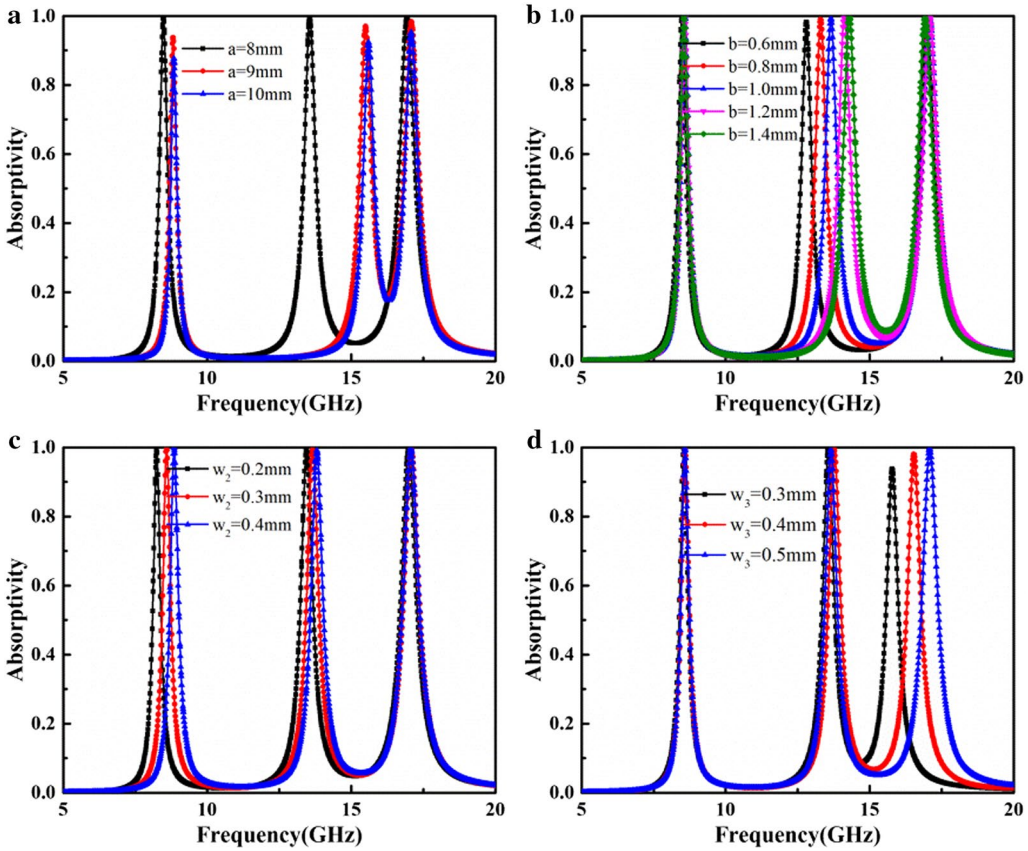

Fig. 6 Absorption spectrum of the MA for different structural parameters: **a** unit periodicity *a*, **b** SRR gap width *b*, **c** MSR ring bar width w_2, **d** 7-shaped patch width w_3

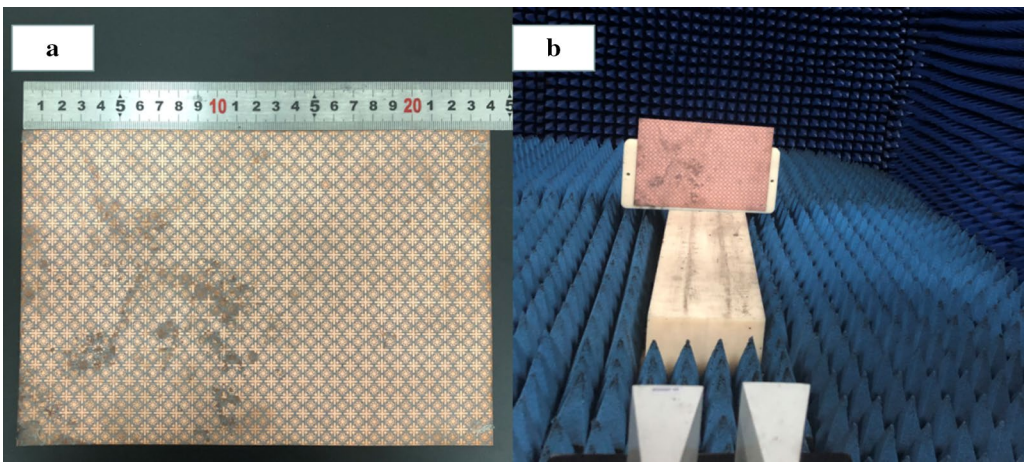

Fig. 7 **a** Fabricated MA prototype. **b** Measurement setup

a increases. The relationship between gap width *b* of the SRR and the absorption spectrum is shown in Fig. 6b. The equivalent capacitance decreases as b increases; thus, the center resonant peak shifts to higher frequencies. However, the lower and upper absorption peaks remain almost unchanged, which provides a convenient way to

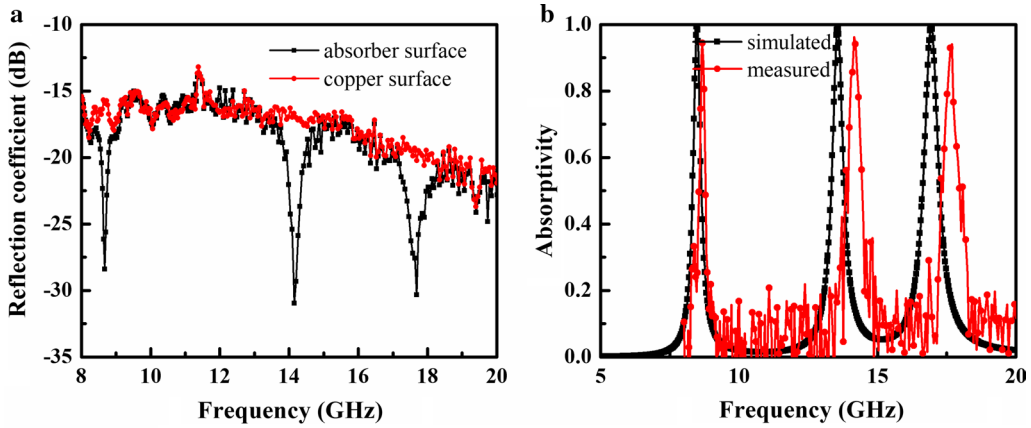

Fig. 8 **a** Reflection coefficient and **b** absorptivity of the MA at normal incidence

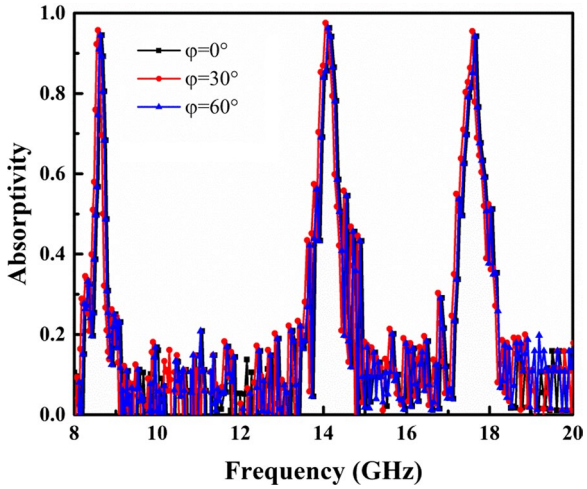

Fig. 9 Measured absorption for different polarization angles under normal incidence

tune individual absorption frequencies. Moreover, the dependence of absorption on the width of the ring bar w_2 is presented in Fig. 6c, where both the lower and center resonant frequencies red-shift as w_2 increases. As w_2 increases, the equivalent capacitance increases because the distance between the SRR and MRR decreases, causing the lower and center resonant frequencies to red-shift. Finally, increasing the bar width w_3 will cause a red-shift in the upper resonant frequency, as shown in Fig. 6d. As the resonant mode is determined by the inner 7-shaped patch, increasing w_3 also increases the equivalent inductance of the inner resonator. Therefore, the resonant frequency exhibits a red-shift.

A 240 mm × 160 mm prototype, corresponding to 20 × 30 unit cells, was fabricated, as shown in Fig. 7a. In the sample preparation, a thin layer of copper was evaporated on the surface of the polyimide, and then the patterns were etched using laser ablation. The measurement

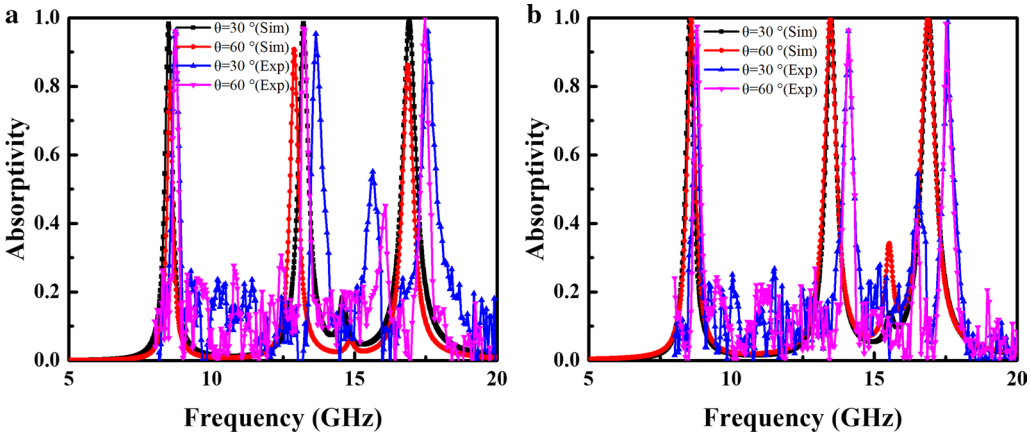

Fig. 10 Simulated and measured absorption for different incident angles: **a** TE and **b** TM polarization

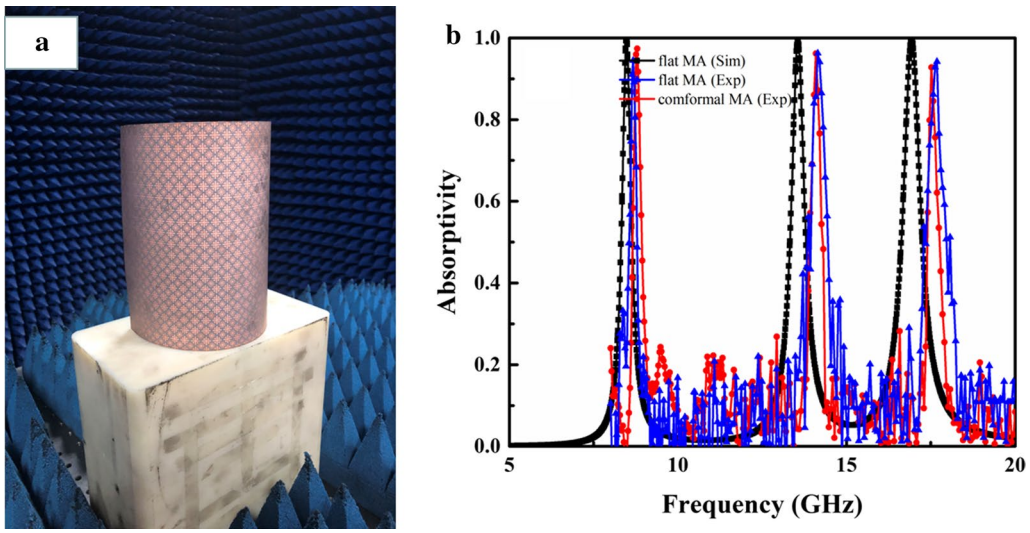

Fig. 11 **a** Flexible absorber attached to a cylinder. **b** Absorption spectra of the flat and conformal MA

setup is shown in Fig. 7b, where absorption in the sample was tested with the free space method. A pair of horn antennas was connected to a vector network analyzer (Rohde & Schwarz ZVA 40) to measure reflection from the sample. The reflection spectrum for a copper plate with the same size as the fabricated sample was measured and used as a reference. The sample was then placed at the same location and the real reflection from the sample was calculated by subtracting the two measured reflected powers. Figure 8a shows the reflection spectrum measured from the copper plate and the fabricated sample, while the absorptivity of the MA is shown in Fig. 8b. The measured absorption is 96%, 97%, and 94% at 8.7, 14.1, and 17.6 GHz, respectively. Compared with the simulation results, the absorption peak frequencies move slightly toward higher frequencies due to manufacturing tolerances and differences in the substrate's permittivity.

Figure 9 shows absorption in the MA measured at different polarization angles of $\phi = 0°$, 30°, and 60°. The result shows that the proposed structure is insensitive to polarization angle. Figure 10 shows the measured absorption spectra for TE and TM polarization when $\theta = 30°$ and 60°. Absorption for both polarizations remains above 95% when $\theta = 60°$ for all absorption peaks.

As mentioned earlier, the proposed MA was fabricated on a highly flexible polyimide film, which can be used in non-planar applications. As shown in Fig. 11a, the absorber was curved and attached to a cylinder with 8 cm radius, and its absorption was then measured. Figure 11b shows absorption spectra for the flat and conformal absorber. It can be observed that the absorptivity of both absorbers is similar. Moreover, peak absorption at the three resonant frequencies was similar before and after bending, which is important in conformal applications.

Conclusion

An ultra-thin, flexible MA with three absorption peaks is presented in this paper. Compared with previous designs, our proposed absorber is ultrathin with total thickness of 0.4 mm, which is approximately 1/88 the free-space wavelength corresponding to the lower absorption frequency. The proposed triple-band absorber exhibits high absorption up to a 60° angle of incidence (above 86% and 99% for TE and TM polarization, respectively). Meanwhile, the symmetry of the structure ensures absorption is insensitive to changes in polarization. An MA with 20×30 unit cells was fabricated and measured for different angles of incidence. The results show that the MA exhibits high absorption at large incident angles. The absorber was fabricated on a flexible polyimide film that can be easily used in the non-planar and conformal applications. The proposed absorber has great potential uses in energy-harvesting and electromagnetic shielding.

Abbreviations

MA: Metamaterial absorber; EM: Electromagnetic; SRR: Split ring resonator; MRR: Modified ring resonator; FDTD: Finite-difference time-domain.

Authors' Contributions
GD conceived the research and wrote the manuscript. KL and HS conducted simulations and measurement, JY, ZY, YL, and XL assisted in processing the data and figures. BC prepared the test sample. All authors read and approved the final manuscript.

Funding
This work was supported by the National Natural Science Foundation of China (No. 61871171, 51803010) and National Key Research and Development Program of China (No. 2018YFB11067005).

Availability of Data and Materials
All data are fully available without restriction.

Competing interests
The authors declare that they have no competing interests.

Author details
[1] Special Display and Imaging Technology Innovation Center of Anhui Province, Academy of Opto-Electronic Technology, Hefei University of Technology, Hefei 230009, China. [2] Process and Mechanical Engineering Technology Laboratory, Space Star Technology Co. Ltd., Beijing 100095, China. [3] 723 Research Institute of China Shipbuilding Industry Corporation, Yangzhou 225101, China.

Received: 4 September 2020 Accepted: 9 November 2020
Published online: 18 November 2020

References

1. Smith DR, Pendry JB, Wiltshire MCK (2004) Metamaterials and negative refractive index. Science 305:788–792
2. Li JY, Bao L, Jiang S, Guo QS, Xu DH, Xiong B, Zhang GZ, Yi F (2019) Inverse design of multifunctional plasmonic metamaterial absorbers for infrared polarimetric imaging. Opt Express 27:8375–8336
3. Seddon N, Bearpark T (2003) Observation of the inverse Doppler effect. Science 302:1537–1540
4. Chen MJ, Wang CX, Cheng XD, Gong CC, Song WL, Yuan XJ, Fang DN (2018) Experimental demonstration of invisible electromagnetic impedance matching cylindrical transformation optics cloak shell. J Opt 20:045608
5. Yi Z, Huang J, Cen CL, Chen XF, Zhou ZG, Tang YJ, Wang BY, Yi YG, Wang J, Wu PH (2019) Nanoribbon-ring cross perfect metamaterial graphene multi-band absorber in THz range and the sensing application. Results Phys 14:102367
6. Lee KT, Kang D, Park HJ, Park DH, Han S (2019) Design of polarization-independent and wide-angle broadband absorbers for highly efficient reflective structural color filters. Materials 12:1050
7. Ghobadi A, Hajian H, Gokbayrak M, Butun B, Ozbay E (2019) Bismuth-based metamaterials: from narrowband reflective color filter to extremely broadband near perfect absorber. Nanophotonics 8:823–832
8. Assimon SD, Fusco V (2019) Polarization insensitive, wide-angle, ultra-wideband, flexible, resistively loaded, electromagnetic metamaterial absorber using conventional inkjet-printing technology. Sci Rep 9:12334
9. Begaud X, Lepage AC, Varault S, Soiron M, Barka A (2018) Ultra-wideband and wide-angle microwave metamaterial absorber. Materials 11:2045
10. Cong LL, Cao XY, Song T, Gao J, Lan JX (2018) Angular- and polarization-insensitive ultrathin double-layered metamaterial absorber for ultra-wideband application. Sci Rep 8:9627
11. La Spada L, Vegni L (2016) Metamaterial-based wideband electromagnetic wave absorber. Opt Express 24:5763–5772
12. Lee D, Hwang JG, Lim D, Hara T, Lim S (2016) Incident angle- and polarization-insensitive metamaterial absorber using circular sectors. Sci Rep 6:27155
13. Landy NI, Sajuyigbe S, Mock JJ, Smith DR, Padilla WJ (2008) Perfect metamaterial absorber. Phys Rev Lett 100:207402
14. Cheng YZ, Yang HL, Cheng ZZ, Wu N (2011) Perfect metamaterial absorber based on a split-ring-cross resonator. Appl Phys A Mater Sci Process 102:99–103
15. Lim D, Lee D, Lim S (2016) Angle- and polarization-insensitive metamaterial absorber using via array. Sci Rep 6:39686
16. Wang LL, Huang XJ, Li MH, Dong JF (2019) Chirality selective metamaterial absorber with dual bands. Opt Express 27:25983–25993
17. Qi LM, Liu C, Shah SMA (2019) A broad dual-band switchable graphene-based terahertz metamaterial absorber. Carbon 153:179–188
18. Wang BX, Tang C, Niu QS, He YH, Chen T (2019) Design of narrow discrete distances of dual-/triple-band terahertz metamaterial absorbers. Nanoscale Res Lett 14:64
19. Wang BX, Wang GZ, Wang LL (2016) Design of a novel dual-band terahertz metamaterial absorber. Plasmonics 11:523–530
20. Luo H, Cheng YZ (2018) Ultra-thin dual-band polarization-insensitive and wide-angle perfect metamaterial absorber based on a single circular sector resonator structure. J Electron Mater 47:323–328
21. Wang BX, He YH, Luo PC, Xing WH (2020) Design of a dual-band terahertz metamaterial absorber using two identical square patches for sensing application. Nanoscale Adv 2:763
22. Appasani B, Prince P, Ranjan RK, Gupta N, Verma VK (2019) A simple multi-band metamaterial absorber with combined polarization sensitive and polarization insensitive characteristics for terahertz applications. Plasmonics 14:737–742
23. Cheng YZ, Cheng ZZ, Mao XS, Gong RZ (2017) Ultra-thin multi-band polarization-insensitive microwave metamaterial absorber based on multiple-order responses using a single resonator structure. Materials 10:1241
24. Wang BX, He YH, Luo PC, Huang WQ, Pi FW (2020) Penta-band terahertz light absorber using five localized resonance responses of three patterned resonators. Results Phys 16:102930
25. Wang BX (2017) Quad-band terahertz metamaterial absorber based on the combining of the dipole and quadrupole resonances of two SRRs. IEEE J Sel Top Quantum Electron 23:4700107
26. Wang BX, Wang GZ, Sang T (2016) Simple design of novel triple-band terahertz metamaterial absorber for sensing application. J Phys D-Appl Phys 49:165307
27. Chen YZ, Zou Y, Luo H, Chen F, Mao XS (2019) Compact ultra-thin seven-band microwave metamaterial absorber based on a single resonator structure. J Electron Mater 48:3939–3946
28. Nourbakhsh M, Zareian-Jahromi E, Basiri R (2019) Ultra-wideband terahertz metamaterial absorber based on Snowflake Koch fractal dielectric loaded graphene. Opt Express 27:32958–32969
29. Ghosh S, Bhattacharyya S, Kaiprath Y, Srivastava KV (2014) Bandwidth-enhanced polarization-insensitive microwave metamaterial absorber and its equivalent circuit model. J Appl Phys 115:104503
30. Petroff M, Appel J, Rostem K, Bennett CL, Eimer J, Marriage T, Ramirez J, Wollack EJ (2019) A 3D-printed broadband millimeter wave absorber. Rev Sci Instrum 90:024701
31. Chen T, Li SJ, Cao XY, Gao J, Guo ZX (2019) Ultra-wideband and polarization-insensitive fractal perfect metamaterial absorber based on a three-dimensional fractal tree microstructure with multi-modes. Appl Phys A Mater Sci Process 125:232
32. Lu WB, Wang JW, Zhang J, Liu ZG, Chen H, Song WJ, Jiang ZH (2019) Flexible and optically transparent microwave absorber with wide bandwidth based on graphene. Carbon 152:70–76
33. Zhao JC, Chen YZ (2016) Ultrabroadband microwave metamaterial absorber based on electric SRR loaded with lumped resistors. J Electron Mater 45:5033–5039
34. Cheng YZ, He B, Zhao JC, Gong RZ (2017) Ultra-thin low-frequency broadband microwave absorber based on magnetic medium and metamaterial. J Electron Mater 46:1293–1299
35. Cheng YZ, Luo H, Chen F (2020) Broadband metamaterial microwave absorber based on asymmetric sectional resonator structures. J Appl Phys 127:214902
36. Wang Q, Cheng YZ (2020) Compact and low-frequency broadband microwave metamaterial absorber based on meander wire structure loaded resistors. Int J Electron Commun (AEÜ) 120:153198
37. Xu JP, Wang JY, Yang RC, Tian JP, Chen XW, Zhang WM (2018) Frequency-tunable metamaterial absorber with three bands. Optik 172:1057–1063
38. Ma B, Liu SB, Bian BR, Kong XK, Zhang HF, Mao ZW, Wang BY (2014) Novel three-band microwave metamaterial absorber. J Electromagn Waves Appl 28:1478–1486

39. Hu FR, Wang L, Quan BG, Xu XL, Li Z, Wu ZA, Pan XC (2013) Design of a polarization insensitive multiband terahertz metamaterial absorber. J Phys D Appl Phys 46:195103
40. Wang BX, Wang GZ, Sang T, Wang LL (2017) Six-band terahertz metamaterial absorber based on the combination of multiple-order responses of metallic patches in a dual-layer stacked resonance structure. Sci Rep 7:41373
41. Deng GS, Xia TY, Yang J, Yin ZP (2018) Triple-band polarisation-independent metamaterial absorber at mm wave frequency band. IET Microw Antennas Propag 12:1120–1125
42. Xu KD, Li JX, Zhang AX, Chen Q (2020) Tunable multi-band terahertz absorber using a single-layer square graphene ring structure with T-shaped graphene strips. Opt Express 28:11482–11492

Publisher's Note